JOURNAL OF CATALYSIS 75, 101–111 (1982)

On the Structure and Selectivity of Graphite-Supported Pt–Ni Alloys

JOSÉ MANUEL DOMÍNGUEZ E.,* ARMANDO VAZQUEZ S.,† ALBERT J. RENOUPREZ,‡ AND MIGUEL JOSÉ YACAMÁN†

*Instituto Mexicano del Petroleo, Eje Central Lázaro Cárdenas, México, D. F., †Instituto de Fisica, U.N.A.M., Apartado Postal 20-364, Delegación Alvaro Obregón, 01000 México, D. F., and ‡Institut de Recherches sur la Catalyse, Villeurbanne, France

Received June 2, 1981; revised December 9, 1981

X-Ray diffraction and transmission electron microscopy were applied to characterize supported Pt–Ni bimetallic systems. It was found that homogeneous alloys were formed. In the cases when the Pt content was greater than 50% the particles have a cubo-octahedral shape. Kinetic results showed that selectivity to isomerization for isopentane increases with Pr content from about 6 to 87% in the composition range between 37 and 100% in atomic Pt. Results are explained on the basis of the variation of percentages of Pt sites present on the (111) faces of the Pt–Ni cubo-octahedrons. A good correlation between B_5-type sites of platinum and selectivity was found assuming that there is no segregation surface on the particle alloys.

INTRODUCTION

Bimetallic systems have been the subject of a number of recent works. In recent years binary alloys composed of metals of VIII and Ib groups were extensively studied (*1–4*). Since the pioneering work of Dowden and Reynolds (*5*) important geometric and electronic effects on the catalytic activity are often reported when two metals are alloyed (*6*). However, very few correlations between structure of alloys and their catalytic activity have been reported. This might be the result of the lack of knowledge about the state of small bimetallic aggregates. The main limitation is that radiational techniques of characterization fail to detect small quantities of metal in diluted systems. Therefore it is not always possible to determine the state of the metal phases and whether they form an alloy or separated phases. A promising alternative is to study alloys with particle size and metal concentration such that the standard characterization techniques can be applied. In this work we study the structure and catalytic properties of Pt–Ni alloys using the neopentane conversion (neo-C_5H_{12}) as a test reaction. In this reaction the metal is the only place for catalytic activity (*7–9*). In addition, the neopentane molecule is isomerized on platinum while on nickel only hydrogenolysis is produced. The determination of the selectivity for isomerization as a function of Pt–Ni alloy composition might provide useful information on the particle surface composition, from which correlations can be sought between selectivity and surface structures.

SAMPLE PREPARATION

Supported platinum, nickel, and platinum–nickel alloys were prepared by deposition from organic solutions of hexachloroplatinic acid ($H_2P_tCl_6 \cdot 6H_2O$) and nickel chloride ($NiCl_2 \cdot 6H_2O$). The substrate was a graphitized carbon: LONZA-LT10 with 99.9% of carbon, a BET surface area of 18 m^2/g, and crystallite sizes above 1000 Å. The method of preparation was that described by Bartholomew and Boudart (*10*). The impregnated supports were evaporated and dried at 100°C in 10^{-5} Torr vacuum and then reduced at 850°C in pure hydrogen. A series of bimetallic catalysts was obtained with atomic compositions ranging from pure nickel to pure platinum with about 10% in weight of total metal. Platinum–

0021-9517/82/050101-11$02.00/0

nickel alloys supported on graphite will hereafter be called GNPX camples, where X means atomic percentage of platinum in the alloy, i.e., GNP50 will mean a Pt–Ni/C catalyst with 50% of Pt.

CHARACTERIZATION OF THE CATALYSTS

The characterization of bimetallic catalysts includes the determination of the alloy formation and homogeneity. This can be carried out by X-ray diffraction without difficulty if total metal concentration is above 5%, as in the present case (*11*). The surface composition can be investigated by adsorption and other standard physical and chemical techniques. It is known that platinum and nickel form a series of solid solutions over all the range of compositions, between 0 and 100% of atomic Pt for the case of bulk material. This system is derived from the theoretical Vegard's law (*12*). The experimental curve gives the variation of the alloy lattice parameter ($\bar{a}$) versus the atomic concentration of individual constituents. From the theoretical curve and the experimental measurements of lattice parameters it is possible to determine the bulk composition. The mean diameters $\bar{D}_v = \lambda/\beta\cos(\theta)$ were determined correcting for instrumental factors. Measurements were performed in a standard diffractometer equipped with a copper tube.

ELECTRON MICROSCOPY

The electron microscopy was performed using the dark field weak beam method of Yacamán and Ocaña (*13*). Samples were tilted in the microscope stage to an optimum visibility condition. Shapes were identified using the weak beam thickness fringes. A Jeol 100-C microscope fitted with special ultra-high resolution pole piece was used. Samples were dispersed in ethanol and placed on 200 mesh copper grids covered with an evaporated carbon. A standard differential flow system coupled with a Varian-1200 chromatograph was used in order to determine the activities of Pt–Ni solids for the neopentane conversion. Measurements at 300 and 360°C were performed using a reactant mixture of pure hydrogen and neopentane (99.9%) diluted in helium (1 to 30). During the reaction the hydrogen to neopentane ratio was always kept equal to 10. Those conditions are similar to the ones used by Boudart and Ptak (*14*). The products of the reaction were light hydrocarbons from C_1 to C_4, plus i-C_4 and i-C_5. The product mixture is separated by means of a 6-m-long column filled with Chromosorb W(80 mesh) impregnated with dimethylsulfolane (20%). A pretreatment at 500°C for 2 hr in pure hydrogen was applied in each case before reaching the reaction temperature (300 and 360°C) and then initial activities after 5 min of reaction were compared.

RESULTS

Table 1 shows the metal concentration on the catalysts as determined by chemical analysis. The values of C_{Pt} and C_{Ni} were always lower than the nominal 10%. Platinum content in atomic proportion was very close to that calculated from X-ray diffraction (XRD) measurements. Table 2 shows the corresponding diameter values for the particles. a_0, a_m, and Δa represent the nominal and measured lattice parameter (in Å) and the difference between those values, respectively. C_{Pt} is the platinum content determined from the lattice parameter values and Vegard's law. The quantities ρ_0, ρ_m, $\Delta\rho$ are the densities and their difference, respectively. The standard deviation ($\Delta\rho/\rho \times 100$) of density for a series of alloys was also determined. This parameter gives an estimation of the degree of nonhomogeneity in the bulk concentration. In the present case this latter parameter is always lower than 2%, meaning that those are small nonhomogeneities and that there is a smooth distribution of densities, and with no aggregates being present observe in Table 2 that C_{Pt} values are close to the ones shown in Table 1, therefore there is a good agreement between both types of measurements.

In Table 3 the mean diameters of crystal-

TABLE 1

Metal Composition in the Alloy as Determined by Chemical Analysis

Sample	GNP0	GNP12	GNP24	GNP37	GNP51	GNP78	GNP100
C_{Pt} (%wt)	0	2.62	4.4	5.55	6.95	8.8	8.5
C_{Ni} (%wt)	8.5	5.5	4.0	3.2	2.0	0.73	0
$C_{Pt} + C_{Ni}$	8.5	8.12	8.4	8.75	8.95	9.53	8.5
C_{Pt} (%atomic)	0	13	25.5	33.3	52.0	79	100

lites are shown for all the alloys and for the pure metals. The parameters were calculated for the (111), (200), and (220) directions. As observed, the best fitting is obtained for the samples labeled GNP100 (pure platinum) and GNP78 (platinum rich alloy). Intermediate alloys have a larger diameter, close to those found for pure nickel. We conclude that platinum–nickel alloys reported in Tables 1 and 2 were homogeneous ($\Delta\rho/\rho > 2\%$) in the bulk and that the presence of platinum in the alloy seems to inhibit the sinterization of the metal, at least for some cases.

The shape of the particles can be directly obtained by weak beam (thickness fringes) electron microscopy of individual particles as described in a previous publication (*15*). The results for the GNP100 catalyst were consistent with our previous findings; the particles tend to have a regular shape which in most cases corresponds to ⟨111⟩ or ⟨110⟩ oriented cubo-octahedron. Typical bright field images for the various catalysts are shown in Fig. 1 and indication of the shape distributions is presented in Table 4. The regular shape of the Pt particles is clearly changed by the alloying with Ni. In fact the

TABLE 2

Characterization of Pt–Ni/C by XRD

	GNP0	GNP12	GNP24	GNP37	GNP51	GNP78	GNP100
a_0 (Å)	3.5306	3.5915	3.6530	3.6972	3.7566	3.8556	3.9281
a_m (Å)	3.5290	3.5920	3.654	3.692	3.758	3.855	3.9250
Δa	0.0016	0.0005	0.0010	0.0052	0.0014	0.0006	0.0031
C_{Pt}	0	12.5	24.8	34.3	51.09	77.34	100
ρ_0	8.9	10.35	1.9	13.5	15.3	18.65	21.45
ρ_m	8.9	10.45	12.0	13.25	15.4	18.55	21.45
$\Delta\rho$	0	0.10	0.10	0.25	0.10	0.10	0
$\frac{\Delta\rho}{\rho} \times 100$	0	0.966	0.840	1.850	0.653	0.536	0

TABLE 3

Mean Diameters of Crystallites

	GNP 0	GNP12	GNP24	GNP37	GNP51	GNP78	GNP100
$\bar{D}_v$ (111) (Å)	444	206	196	346	394	103	153
$\bar{D}_v$ (200) (Å)	357	166	147	297	298	91	127
$\bar{D}_v$ (220) (Å)	398	134	102	228	215	66	137

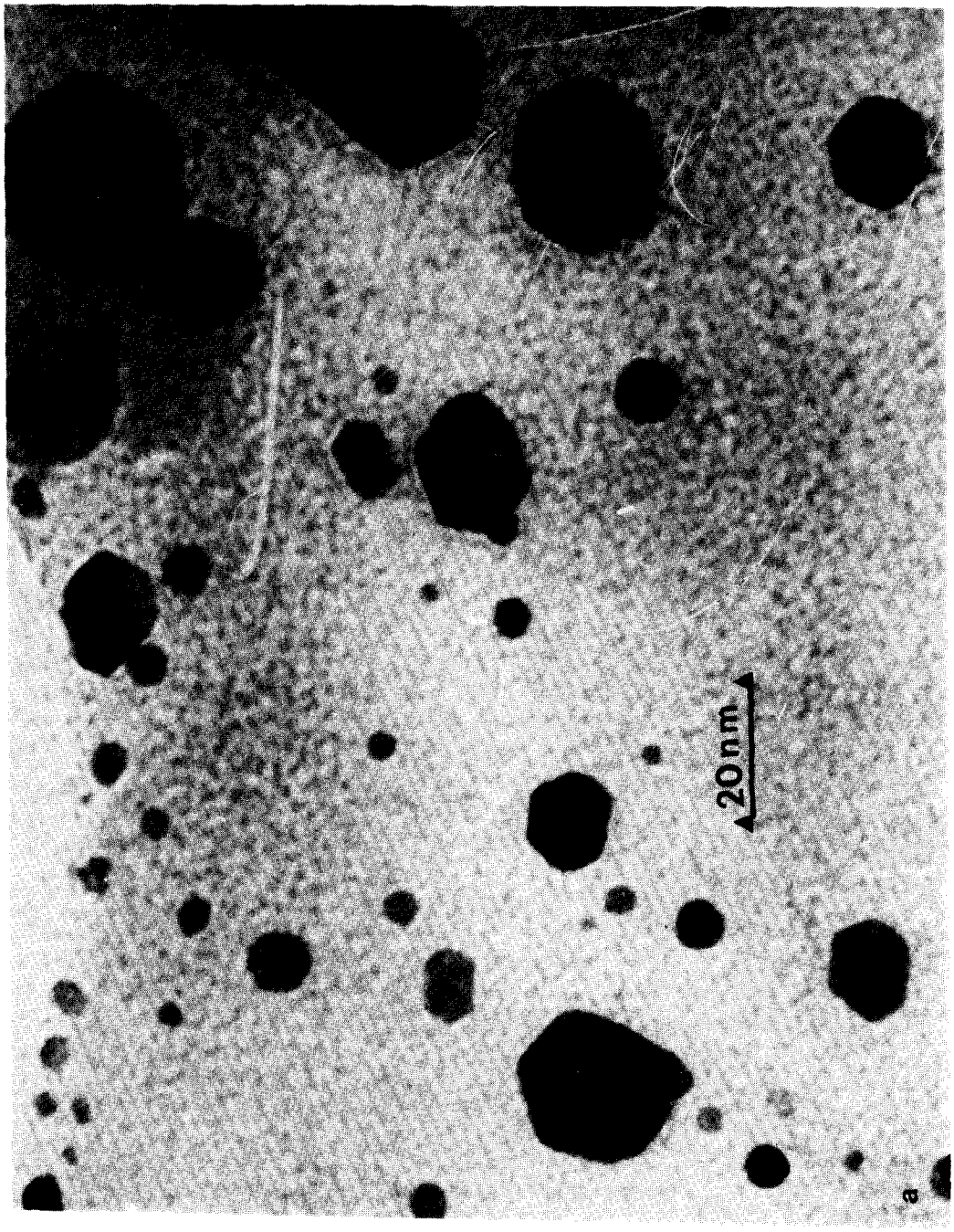
20nm
a

FIG. 1. Bright field images of Pt–Ni catalyst at different compositions (see the text for notation). (a) GNP100, (b) GNP75, and (c) GNP15.

FIG. 1—*Continued.*

TABLE 4

Shape Distributions for Different Particles Taken from a Sample of 1000 Particles Each Case

Catalyst	Fivefold (%)	Cubo-octahedral ⟨111⟩ oriented (%)	Cubo-octahedral ⟨110⟩ oriented (%)	Irregular shape or spherical (%)
GNP100		44	32	24
GNP78		26	13	61
GPN12	10			90
GNP100	2			98

pure Ni catalyst tends to form predominantly irregular particles. As the concentration of Ni increases the number of multiple or single-twinned particles starts to become significant.

In order to use the TEM techniques to quantify the surface sites it is necessary to use the weak beam images. Figure 2 shows an example of the fringe profile obtained for a cubo-octahedral ⟨111⟩ particle; the fringe profile shows that the particle is truncated at 40% of its height as indicated in the inset of the figure; with this shape the effective area of the top ⟨111⟩ surface exposed to a gas will be higher than in the normal case. An accurate counting of the surface sites requires taking these effects into consideration.

In order to check the homogeneity of the alloy for small particles (<50 Å) two TEM techniques were used: the defocused method of Yacamán *et al.* (*16*) and the single-particle diffraction using a STEM-Jeol 100CX microscope. In the microdiffraction pattern the graphite spots were used for internal calibration of the diffraction cam-

FIG. 2. Weak beam thickness fringes for a hexagonal particle which shows that the shape corresponds to a truncated cubo-octahedron.

era length and a higher accuracy was achieved in the determination of the lattice constant. As a general case the alloys were found to be homogeneous. In a few cases some surface segregation with Ni completely precipitated to the surface was detected as reported in a previous work (*17*). However, for the statistical counting of surface sites those particles were not significant and represented isolated cases.

Pure platinum on graphite forms hexagonal profile particles in the size range between 20 and 250 Å. This profile corresponds to a cubo-octahedron in three dimensions bounded by (111) and (100) faces.

Platinum-rich alloys (i.e., Pt_{78}–Ni_{22}/C) are formed mainly by cubo-octahedral-shaped particles and in a smaller proportion by irregular, triangular, and square shapes.

Nickel-rich alloys (i.e., Pt_{12}–Ni_{88}/C) exhibit many irregular shapes and a lower proportion of spherical and fivefold decahedral and icosahedral shapes.

KINETIC RESULTS

The activities and selectivities of Pt–Ni/C catalysts for hydrogenolysis and isomerization of neopentane (neo-C_5H_{12}) were measured with a reactant gas mixture of H_2/neopentane = 10, at 300 and 360°C, respectively. The following kinetic parameters were measured:

The percentage of hydrogenolysis products (θ_i) which is the ratio between the partial pressure of product i and the sum of hydrogenolysis products ($\theta_i = 100 \times P_i/\Sigma_i P_i$ where P_i represents the product partical pressures).

The selectivity of isomerization (S_i), defined as the ratio between the isopentane proportion with respect to the total conversion.

The specific activities for hydrogenolysis (V_s^H) and isomerization (V_s^i) and the fission parameter M defined as $\Sigma\ C_i(5 - i)/C_1$ which takes into account the possible successive demethylations. If $M > 1$ the cracking path goes through primary reactions only. If $M > 1$ secondary reactions like $C_3 \rightarrow C_2 \rightarrow C_1 \rightarrow 3C_1$, or $C_4 \rightarrow C_3 + C_1 \rightarrow C_2 + 2C_1$ $4C_1$ are important.

The results are shown in Tables 5 and 6. At 300°C the main product of hydrogenolysis is methane whose proportion decreases slowly as the platinum content increases. Simultaneously there is an apparent increase in isobutane content. This is probably because incorporation of platinum to the alloy causes a reduction in the multiple hydrogenolysis mechanism. For nickel-rich alloys with 24 and 21% of Pt (GNP24, GNP12) the proportion of methane increases as that of isobutane reaches a minimum.

Apparently those alloys are more active

TABLE 5

Kinetic Measurements for Pt–Ni Alloys[a]

Cracking	GNP0	GNP12	GNP24	GNP37	GNP51	GNP78	GNP100
θ_1[b]	50.5	45.3	72.8	52.1	40.2	41.1	43.0
θ_2[b]	23.7	16.0	10.7	16.3	18.9	19.3	13.5
θ_3[b]	14.6	16.4	6.6	20.1	23.3	5.9	12.3
θ_4[b]	10.9	22.1	9.83	11.2	17.4	33.5	31.1
V_s^H (10^8 mol s^{-1} g^{-1})	0.38	4.5	7.0	2.6	3.17	5.3	7.6
M	2.21	2.27	0.76	1.93	3.0	2.51	2.24
S[c]	0	0	0	29.8	55.9	77.4	87.2
V_s^i(10_8 mol s^{-1} g^{-1})	0	0	0	1.09	4.02	18.2	51.8

[a] T = 300°C; H_2/neop = 10.

[b] Percentages with respect to the total conversion in hydrogonolysis products (C_1, C_2, C_3, i-C_4).

[c] Percentage with respect tot the total conversion (hydrogenolysis + isomerization).

TABLE 6

Kinetic Measurements for Pt–Ni Alloys[a]

	GNP0	GNP12	GNP24	GNP37	GNP51	GNP78	GNP100
C_1 $(\theta_1)^b$	78.5	87.8	71.9	53.1	44.0	41.9	50.7
C_2 $(\theta_2)^b$	16.6	10.1	23.3	16.0	18.1	21.7	14.9
C_3 $(\theta_3)^b$	2.2	1.4	3.6	11.0	12.7	15.9	16.5
i-C_4 $(\theta_4)^b$	2.5	0.4	1.97	19.7	25.0	20.3	17.8
V_s^H	3.11	359	112	12	21.4	35	15 (10^8 mol s^{-1} g^{-1})
M	0.73	0.39	1.09	1.69	2.38	2.89	1.88
-i-C_5 $(S)_i$	0	0	0	32.2	45.9	56.8	82.8
V_s^I	—	—	—	5.8	18.2	46.0	72.1 (10^8 mol s^{-1} g^{-1})

[a] T = 360°C; H_2/neo-C_5H_{12} = 10.

[b] With respect to the total conversion in hydrogenolysis (C_1, C_2, C_3, i-C_4).

by a factor of 10 for hydrogenolysis than pure nickel at 300°C and by a factor of 100 at 360°C. For those nickel-rich solids the parameter M goes through has a minimum value. The observed increase in activity has been also reported by Nowak and Koros (*18*) for bimetallic Pt–Ni catalysts. In addition, at 360°C methane production increases substantially. For pure nickel and nickel-rich alloys the fission coefficient is lower than one, and thus secondary reactions occur. However M increases with the platinum concentration starting when this is larger than 25%. At a Pt concentration greater than 50% the production of isobutane increases while that of methane de-

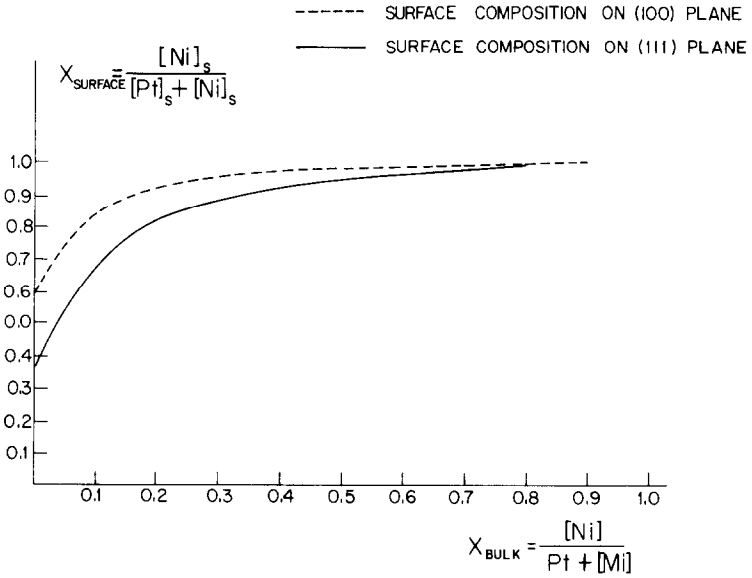

FIG. 3. Surface composition of Pt–Ni particles as a function of concentration as predicted by the solution theory.

creases. At 360°C the proportion of C_2 and the C_3 proportion becomes slightly reduced indicating probably that a small portion of C_3 produced by cracking of the neopentane molecule goes to C_2 and C_1 at least for the platinum-rich alloys and the GNP37 sample. It is also observed that the isomerization rate drops to zero for catalysts containing less than 25% Pt. Alloys with 37% or more Pt have an isomerization rate which increases with the content of platinum, going from 1 to 72 molec/s-g at 360°C, respectively. The corresponding selectivity of isomerization S_i increases from 0 to more than 80% at 300 and 360°C, respectively, in the composition range between 25 and 100% at-Pt. Results for the selectivity are summarized in Fig. 3 as a function of alloy composition at 300 and 360°C.

DISCUSSION

It is not possible to determine directly the surface composition in the bimetallic particles.

However simple models can be assumed in order to understand the kinetic results. If the solution theory Burton and Machlin (*19*) is assumed valid then a nickel-enriched surface will be expected because the heat of sublimation of nickel (102.8 kcal/mol) is smaller than that of platinum (135 kcal/mol). Figure 3 shows a calculation of the expected surface concentration of Ni.

The results show that the isomerization properties of the alloys decreased when the number of cubo-octahedral particles decreased. It is reasonable to assume that the isomerization occurs in triplets of atoms (B_3 sites in the van Hardeveld and Hartog (*20*) notation) present in ⟨111⟩ surfaces; when Ni atoms are incorporated to the surface the number of B_3 Pt sites decreases and the isomerization properties are deteriorated. Using the calculations of Ref. (*25*) and the data of Fig. 3 it is possible to calculate the total number of B_3 sites for the 100 and 150 Å cubo-octahedral as a function of the Ni concentration. In Fig. 4 the concentration

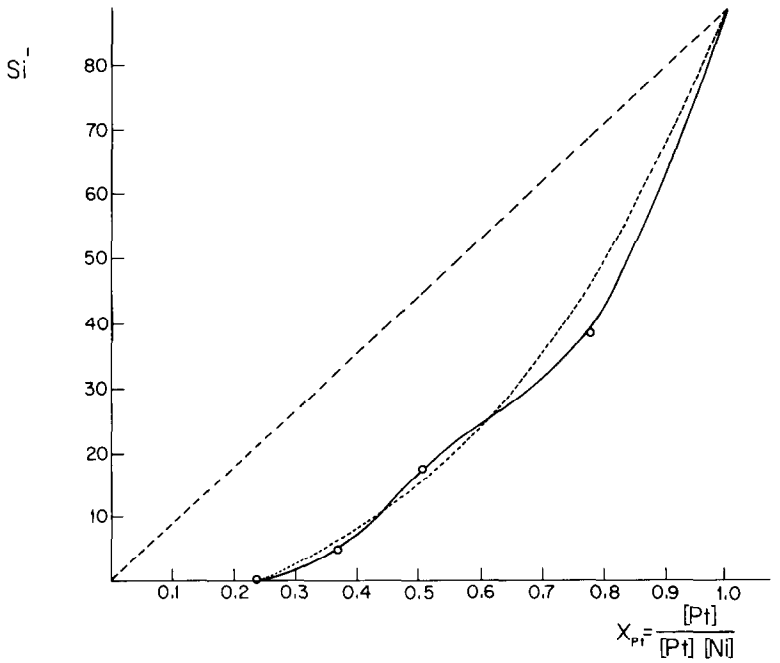

FIG. 4. Variation of reduced selectivity, defined as $S_i = S_{Pt-Ni}/S_{Pt}X_{Pt}$ where S_i is the measured selectivity of particle i and X_P is the concentration, and of the B_1 sites (---) and B_3 sites (. . .) as function of alloy composition.

of B_3 sites is plotted along with the experimental selectivity curve. There is a good agreement between the two curves in the same figure; it is possible to see that the total number of one Pt site has a large deviation with the experimental curve calculations of B_3 fractions and their correlation with selectivity implies that: (i) only hexagonal cubo-octahedral particles contributed to isomerization by providing (111) planes exposed to reactant gases; (ii) irregular outlined particles have very little influence in the isomerization reaction; (iii) external particle facets are smooth; and (iv) the sticking coefficient of reactant molecules is very small, thus providing a high probability of finding "free sites" for isomerization. With these assumptions the activity results can be qualitatively understood; a more quantitative explanation will require more detailed information on the surface structure of the particle.

ACKNOWLEDGMENTS

We appreciate discussions with Dr. K. Klier and Dr. S. Fuentes. We also thank Dr. B. Moraweck from the IRC-CNRS of Lyon, France, for assistance in preparation of samples and Mr. F. Ruíz for technical assistance during the electron microscopy studies. Part of this work was supported by the PNCB-CONACyT program.

REFERENCES

1. U.S. Patent No. 2,848,377.
2. Ponec, V., and Sachtler, W. M., II, *J. Catal.* **24,** 250 (1972).
3. Lam, Y. L., and Boudart, M., *J. Catal.* **50,** 530 (1977).
4. Sinfelt, J. H., *Accounts Chem. Res.* **10,** 15 (1977).
5. Dowden, D. A., and Reynolds, P., *Discuss. Faraday Soc.* **8,** 184 (1950).
6. Sinfelt, J. H., Carter, J. L., and Yates, D. J. C., *J. Catal.* **24,** 283 (1972).
7. Anderson, J. R., and Avery, N. R., *J. Catal.* **7,** 315 (1967).
8. Boudart, M., Aldag, W., Ptak, L. D., and Benson, J. E., *J. Catal.* **11,** 35 (1968).
9. Rooney, J. J., *J. Catal.* **58,** 334 (1979).
10. Bartholomew, C. H., and Boudart, M., *J. Catal.* **25,** 173 (1972).
11. Domínguez, J. M., Doctoral Thesis, Univ. Claude Bernard, Lyon, France (1977).
12. Allison, E. G., and Bond, G. C., *Catal. Rev.* **7,** 233 (1972).
13. Yacamán, M. J., and Ocaña, T., *Phys. Stat. Sol.* **A47,** 571 (1977).
14. Boudart, M., and Ptak, L. D., *J. Catal.* **16,** 90 (1970).
15. Yacamán, M. J., and Domínguez, J. M., *J. Catal.* **64,** 213 (1980).
16. José Yacamán, M., Contreras, J. L., and Zenith, J., *Appl. Surface Sci.* **6,** 71 (1980).
17. José Yacamán, M., Domínguez, J. M., and Fuentes, S., *Surface Sci.* **106,** 472 (1981).
18. Nowak, E. J., and Koros, R. M., *J. Catal.* **7,** 50 (1967).
19. Burton, J. J., and Machlin, E. S., *Phys. Rev. Lett.* **37,** 21, 1433 (1976).
20. Van Hardeveld, R., and Hartog, F., *Surface Sci.* **15,** 189 (1969).